



Modelling wetland methane emission estimates by leveraging new observations of anthropogenic point-source plumes

Anthony Campbell^{1,2}, Lauren Potyk^{1,3}, Benjamin Poulter^{4,^}

- 5 ¹ Biospheric Sciences Laboratory, Goddard Space Flight Center, NASA, Greenbelt, MD, USA
 - ² Goddard Earth and Technology Research II, University of Maryland, Baltimore County, Baltimore, MD, USA
 - ³ John A. Paulson School of Engineering and Applied Sciences, Harvard University, Cambridge, MA, USA
 - ⁴ Spark Climate Solutions
 - ^ formerly at: Biospheric Sciences Laboratory, Goddard Space Flight Center, NASA, Greenbelt, MD, USA
- 10 Correspondence to: Anthony Campbell (anthony.d.campbell@nasa.gov)

Abstract.

Satellite retrieval capabilities for detecting methane (CH₄) diffuse and point sources have increased drastically over the last decade. These observations are playing an important role in atmospheric inversion systems to optimize emissions from anthropogenic and natural sources. A critical component of atmospheric inverse modelling is the prior estimate of CH₄ emissions, which impact both the magnitude of posterior emissions and the distribution between sectors, including wetland emissions. Here we utilize point source retrievals from GHGSat to update prior emission estimate for fossil fuels. We demonstrate the effect on posterior emission using the Integrated Methane Inversion for the Western Siberian Lowlands. The updated GHGSat-informed fossil prior results in a reduction in wetland CH₄ flux of 0.59 Tg CH4 yr⁻¹. The approach demonstrates the potential impact of large point sources, that are typically not accounted for in bottom-up emission inventories. Due to modelling approaches adjusting anthropogenic and natural sources at the state vector level, input proportion of these sectors is critical for understanding regional methane budgets and the effect of climate change on wetland emissions.

1 Introduction

Methane (CH₄) is a greenhouse gas, approximately 80 times as potent as CO₂ over 20 years, with a short atmospheric lifespan of approximately nine years, making it a target for climate mitigation efforts (Shindell et al., 2024). Aquatic and wetland ecosystems generate up to half of global CH₄ emissions (Rosentreter et al. 2021). These natural CH₄ emissions are potentially increasing with warming (Peng et al. 2022, Zhang et al., 2023). Remote sensing approaches are critical for improving monitoring, reporting, and mitigation of CH₄ emissions (Conrad et al., 2023). New technologies and the deployment of satellite constellations are increasing our ability to monitor super-emitters from various point sources, e.g., oil, gas, coal mines, landfills, and agriculture (Jervis et al. 2020). The capacity for satellite-based remote sensing of these point-sources has increased significantly over the past two years with many satellites launching and entering operational



35

40

45

50



status (GHGSat, NASA EMIT, GaoFen-5, MethaneSat, CarbonMapper; Jacob et al. 2022; He et al. 2024). While these approaches are limited to high concentration anomalies from anthropogenic sources, the data can be combined with atmospheric inversions to improve estimations of natural sources.

1.1 Challenges in separating wetland and anthropogenic CH₄ emissions

In this study, we develop an approach to incorporate point source emissions into an atmospheric inversion model to improve estimates of wetland emissions for the Western Siberian Lowlands (WSL). In situ observations in WSL show CH4 emissions from permafrost increasing during the thaw season (Rößger et al. 2022). However, ground measurements are sparse due to the region's large extent and remoteness. Globally, we calculated overlap with wetlands and waterbodies and oil and natural gas fields using the Oil and Gas Infrastructure Mapping dataset (OGIM 1.1) and the Global Lake and Wetland Dataset (GLWD 2.0; Omara et al. 2023; Lehner 2024; Figure S1). We found that 75% of oil and natural gas fields are co-located with wetlands or water and on average 35% (SD: 41%) of oil and natural gas field area were wetland land cover. In Russia this rises to 98% of oil and natural gas fields are co-located with wetlands and an average of 73% (SD: 38%) of oil and natural gas fields were wetlands. In the WSL, wetlands and oil and gas facilities are highly likely to overlap. Wetland CH₄ emissions are diffuse, meaning that the emissions at any one location are very low compared to point sources. Still, if the wetland areas are large their emissions can result in a considerable integrated flux per region. Therefore, modelling and satellite observations are necessary to understand regional CH₄ flux. Wetland CH₄ emissions are estimated using a 'forward model', i.e., land-surface model that predicts emissions, or from an 'inverse model' using atmospheric inversions. Both approaches have large uncertainties due to limited data. Atmospheric inversions require a priori information on anthropogenic and natural emission sources with the large uncertainty of these estimates affecting the posterior flux estimates. Improving the prior flux estimate for anthropogenic sources using point source emissions data could thus potentially improve the posterior estimate of wetland emissions.

Russian oil and gas sector CH₄ emissions from atmospheric inversions are highly uncertain due to differing reporting methodologies, low observation density, and high variability between inventories (Shen et al. 2023). These emissions are estimated using either country-reported emissions to the United Nations Framework Convention on Climate Change (UNFCCC) that are spatially distributed to oil and gas infrastructure in databases such as the Emission Database for Global Atmospheric Research (EDGAR) and the Global Fuel Exploitation Inventory (GFEI), or by groups such as Climate TRACE. GFEI and EDGAR use the best available geospatial data to estimate the spatial distribution of emissions from various sectors, for example, oil refineries (Janssens-Maenhout et al. 2013; Scarpelli et al. 2022). For 2019, GFEI v2 has slightly lower oil, gas, and coal emissions compared to EDGAR v6.0 (Scarpelli et al. 2022). Some of the oil and gas infrastructure locations in Russia are restricted from the public domain (Omara et al. 2023). The uncertainty and lack of data completeness increase the likelihood of under attributing emissions to the oil and gas fields of the WSL, resulting in over attribution of emissions to natural sources such as wetlands. The Integrated Methane Inversion (IMI) provides a unified modelling framework for optimizing modelled CH₄ emissions with TROPOMI Methane (XCH₄) total column Level 2 data product

https://doi.org/10.5194/egusphere-2025-5398 Preprint. Discussion started: 26 November 2025

© Author(s) 2025. CC BY 4.0 License.



70



(Copernicus Sentinel-5P, 2021; Varon et al. 2022a). The relative contribution of CH₄ from different sectors is consistent between the prior and posterior emission estimates. Total annual emissions are optimized based on the TROPOMI XCH₄ observations. Therefore, if the proportion of emissions from sectors in a state vector element is incorrect, that would result in sectoral misattribution of emissions. This makes the distribution and relationship between sectors critical especially in regions with multiple high emission sectors such as the WSL.

1.2 GHGSat to inform CH4 inversions

In this study, we use GHGSat data, a commercial satellite constellation that monitors super emitters, i.e. the less than 20% of sources which account for greater than 60% of emissions, across the globe (Brandt et al. 2014; Duren et al. 2019). GHGsat uses a Fabry–Pérot imaging spectrometer to monitor CH₄ absorption bands in the short-wave infrared (SWIR; Jacob et al. 2022; Jervis et al. 2021). Independent verification studies show GHGSat satellites have an emissions detection threshold of between 100-200 kg CH₄ hr⁻¹, depending on the observation conditions (McLinden et al. 2024). In a controlled release study GHGSat detected a 400 kg CH₄ hr⁻¹ plume (Sherwin et al. 2024). We develop a methodology to update regional oil and gas priors with plume measurements from GHGSat. We apply our approach to the WSL, a region with extensive wetlands and oil and gas production.

30 2 Methodology

A database of GHGSat observations for the Western Siberian Lowlands (WSL) is developed and used to estimate prior anthropogenic emissions for the region. The updated emissions are derived from the GHGSat emission and geospatial information on the distribution of oil and gas infrastructure in the region. These updated emissions are incorporated into the IMI model and compared to default model simulations to determine the effect that unobserved emissions could be having on anthropogenic and wetland emissions in the region.

2.1 Study site

85

The WSL is a region of Russia with an estimated peatland extent of 592,440 km² and storing 70.21 Pg C in a mix of wetland and permafrost soils (Sheng et al. 2004). The region is important in the global carbon cycle, with a yearly emission from permafrost lakes estimated at 12 ± 2.6 Tg C yr¹ (Serikova et al. 2019). The WSL is within the Urals Federal District which is responsible for the majority of oil and gas production in Russia (Suslov et al. 2019). Russia is the second largest emitter of fugitive CH₄ emissions from oil and gas (Solazzo et al. 2021) with ultra-emitters (>25,000 kg hr¹) estimated to represent between 10% and 20% of annual reported oil and gas emissions (Lauvaux et al. 2022). We define the domain with a bounding box of 60.0°E, 66.0°E to 70.0°N to 79.1°N for a total area of 446,730 km². The IMI model setup includes optimizing the boundary conditions, for 4° around each of the 4 sides of the domain. The core domain includes the three

GHGSat observation sites (Figure S2)



100

105

110

115

120

125



2.2 Integrated Methane Inversion Model:

We use the IMI model, based on Goddard Earth Observing System (GEOS)-Chem (Henze et al. 2007; https://doi.org/10.5281/zenodo.4618180) and the Harmonized EMissions Component module (HEMCO; Lin et al. 2021). The chemical transport (CTM) model is optimized with TROPOMI XCH₄ using an analytical minimization of a leastsquares Bayesian cost function (Varon et al. 2022a). This results in accuracy metrics such as Root Mean Square Error (RMSE) and bias comparing the prior representing the CTM before optimization and the posterior representing the estimate following the optimization process. The priors for global modelling included in the IMI are 1) EDGAR v6.0 (Ferrarioet al. 2021), 2) Global Fuel Exploitation Inventory (GFEI v2.0, Scarpelli et al., 2022), 3) geological seeps (Etiope et al. 2019), 4) fires (Randerson et al. 2018), 5) termites (Fung et al. 1991), 6) wetland fluxes from WetCHARTS (Bloom et al., 2017). To update these priors to include an estimate of fugitive emissions, we acquired GHGSat emission rates, a level 4 data product, as part of the NASA Commercial Satellite Data Acquisition onboarding review for the sensor. We downloaded data from the GHGSat platform SPECTRA (spectra.ghgsat.com/map). We requested GHGSat images for areas where oil and gas facilities are co-located with wetlands, specifically, the North Slope of Alaska, the Mississippi Delta, the Sudd Wetlands, the Niger Delta, and the Western Siberian Lowlands (WSL; Table S1). For this analysis, we used a total of 40 images acquired over all three sites in the WSL (Figure 1). The GHGSat constellation (in total, 12 satellites) targeted the three sites which each included multiple oil and gas facilities. GHGSat acquired at least ten images for all sites (n=13, 16, and 11). Sites 2 and 3 had images with multiple plumes within a single image (Table S2).

2.3 Updating oil and gas priors:

To update the oil and gas priors, we created a fugitive emissions distribution and combined that with the GFEI v2.0 fossil fuel prior. To create the spatial distribution of fugitive emissions, we used a combination of GHGSat plume emissions and oil and gas flaring detections from OGIM (Omara et al. 2023) extrapolating GHGSat emission estimates to oil and gas infrastructure locations which were not observed in our GHGSat survey (Figure S3). The GHGSat plume detections were assumed to represent a statistical sample of leaking infrastructure that can be extrapolated to all oil and gas facilities in the region. In the WSL, we observed 20 plumes for the 40 image acquisitions, including three images with two plumes from two different facilities (Table S2). Satellite acquisitions targeted three areas of the Western Siberian Lowlands from July 2023 to April 2024 as part of the NASA CSDA Programs assessment of GHGSat. We utilized the *propagate* package (Spiess 2018) in R Statistical Software 3.6.3 (R Core Team, 2021) to estimate the annual CH₄ emissions for all flaring location. The error propagation Eq. (1) combined emissions, emission error, and likelihood along with each terms associated uncertainty (Eq 1): (*Emissions* ± *Error*) × *Likelihood*,

Emissions and errors were calculated from the reported plume emission rates and associated uncertainty (Table S2). To calculate the emission likelihood, we identified all oil and gas infrastructure within each GHGSat footprint from high resolution imagery and considered occurrence for each of those facilities during each image collection. The errors of these



135



three terms were combined using 100,000 Monte Carlo simulations. We converted the result into kg CH₄ per second (kg CH₄ s⁻¹). We then used flaring detections from the OGIM to constrain our potential facility locations for updated emissions (n = 869; Figure 1), including locations within the domain and those within the 4° boundary region. We estimated the annual emissions for each of the 869 sites using a normal distribution of the mean and standard deviation from the Monte Carlo simulations (Figure 2). Any negative values resulting from this prediction were assumed to be zero emissions, i.e., non-occurrence. We converted these values into a NetCDF file and incorporated this updated prior into the IMI as an additional fossil fuel emissions in the oil and gas prior estimate (Figure 2).

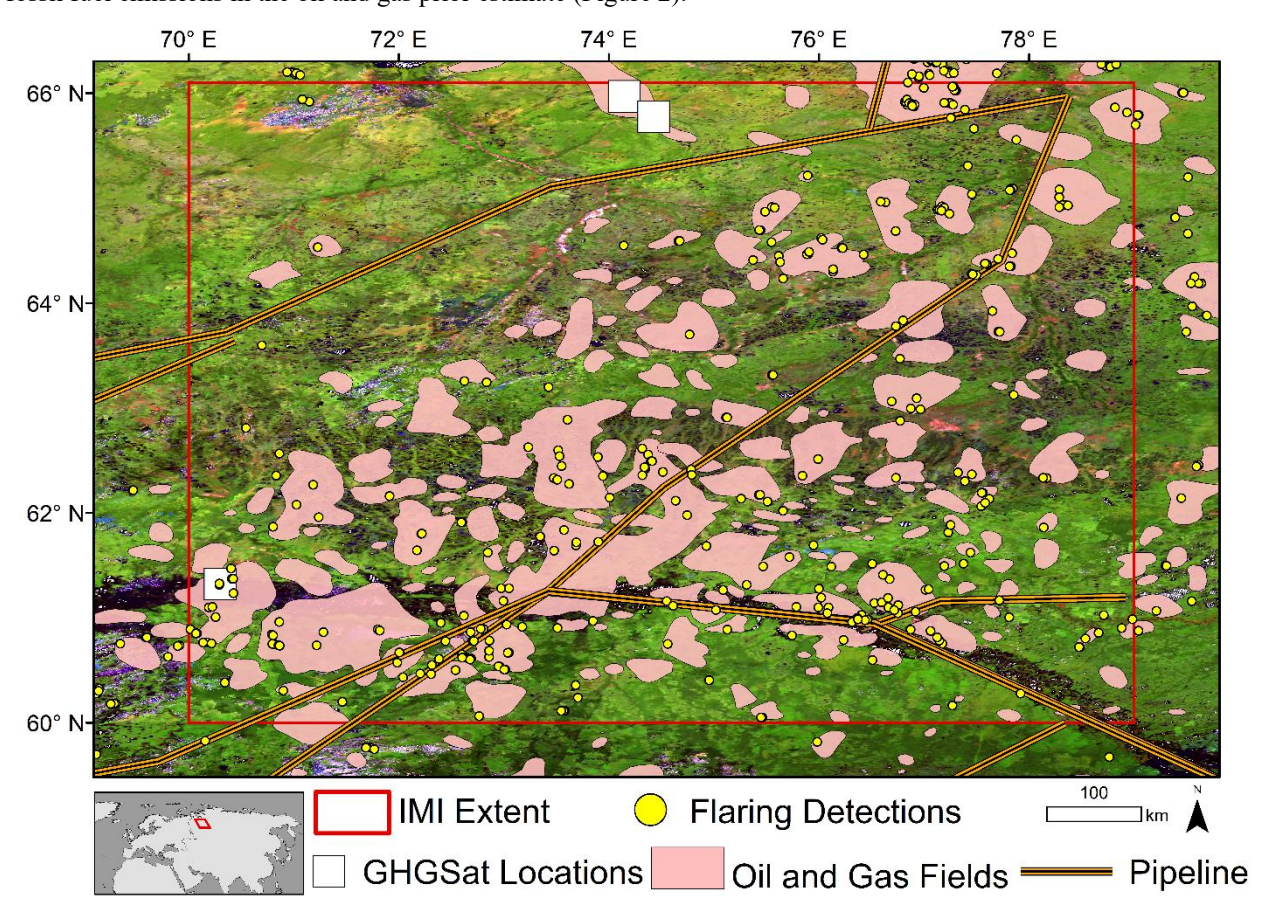


Figure 1. Oil and Gas infrastructure represented by gas flaring, oil and gas field extent, and pipeline locations for the WSL from the OGIM (Omara et al. 2023). The domain of the IMI model is in red and includes both all three GHGSat sites. MODIS surface reflectance composite displayed using R = band 7 (2105-2155 nm), Green = band 5 (1230-1250 nm), and Blue = band 3 (459-479 nm).



145

150



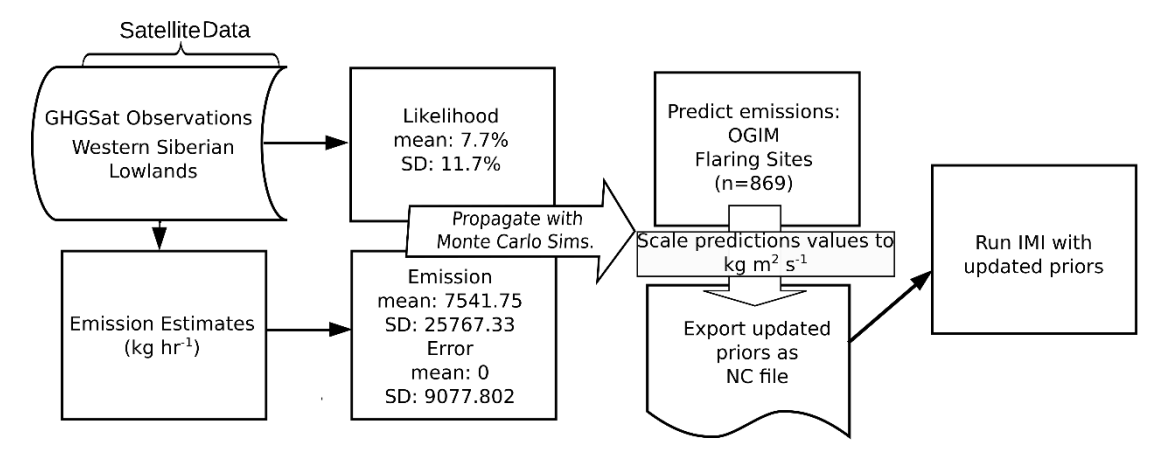


Figure 2. The workflow for updating oil and gas priors with GHGSat from plume observations.

2.4 Integrated methane inversion (IMI) model runs

The IMI v1.2.1 was run following standard methods on Amazon Web Services (AWS) (Varon et al. 2022a; Varon et al. 2022b). We ran a default model (with GFEI v2.0 fossil fuel priors) and another model with GHGSat informed priors, subsequently referred to as the default and updated models, respectively. The IMI uses GEOS-Chem, a chemical transport model, as the forward model to constrain CH₄ fluxes based on the coal, oil, and gas priors from GFEI v2.0 and other anthropogenic priors from EDGAR v6.0 (Varon et al. 2022a).

We ran the model from 01/06/2021 to 31/07/2021. We ran a nested grid simulation for the WSL region (70.0-79.0° E and 60-66.1° N). This domain resulted in a total of 733 state vector elements at a 0.25° x 0.3125° spatial resolution which, were clustered into 100 elements. The different priors would result in each model having unique state vector clusters. To control for this variability, we used the state vectors from the updated model for both model runs. All other parameters were set to the default except the updated model, which included the GHGSat-derived emission layer in the priors.

3 Results

The average CH₄ emission from the GHGSat plume detections was 7,541± 25,767 kg CH₄ hr⁻¹. The smallest observed plume had a rate of 378 kg CH₄ hr⁻¹. The median of our observed plumes was 946 kg CH₄ hr⁻¹. The largest observed emission was 116,739 kg CH₄ hr⁻¹ in site 1, which was one of only two plume observations at that location (Table 1). In contrast, site 3 had consistent smaller magnitude plumes in all but one image. At site 3, emissions averaged 2,124 ± 2,082 kg CH₄ hr⁻¹. The observation on 20/04/2024 was site 3's second-largest observation (Figure 3).





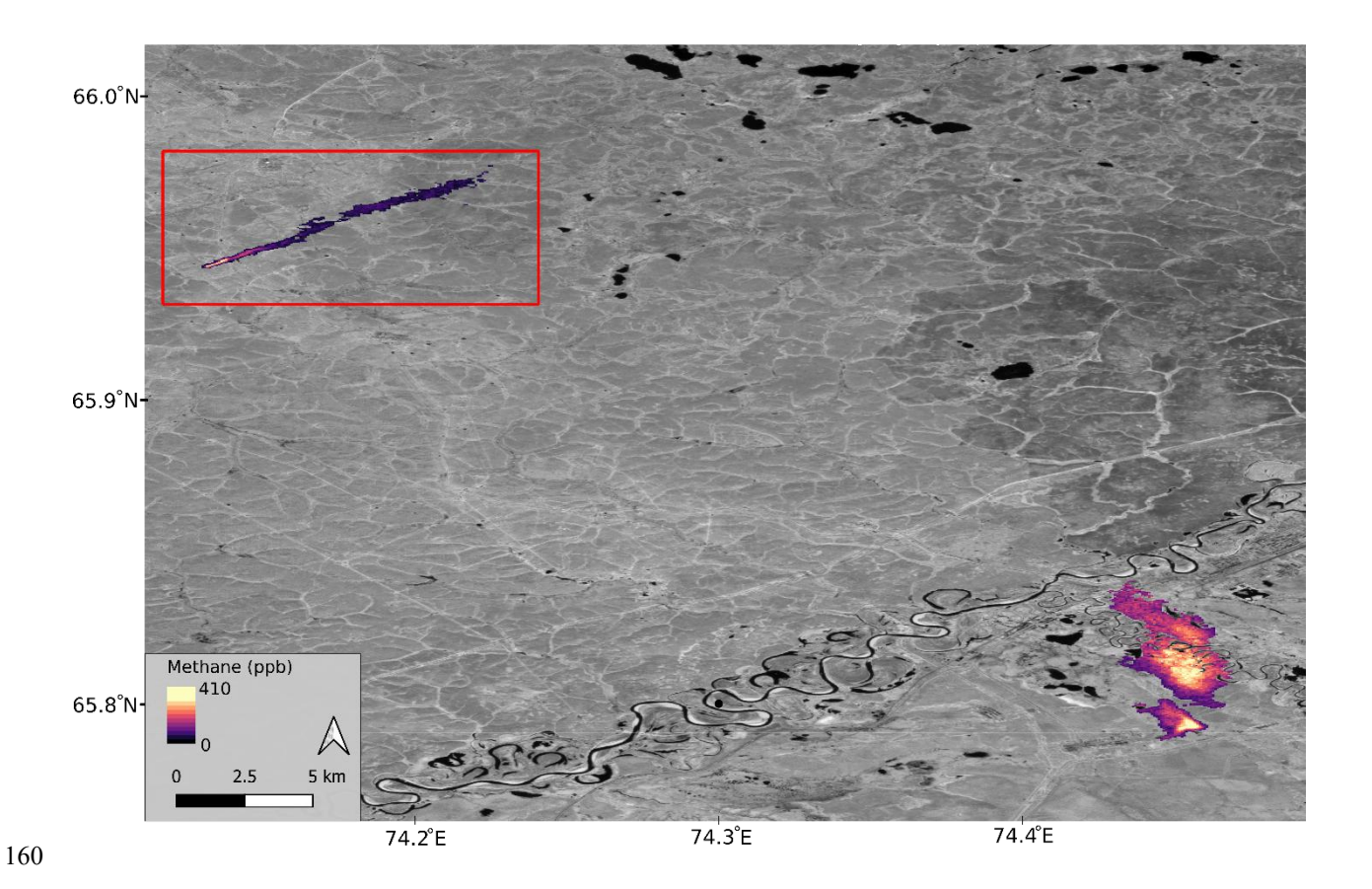


Figure 3: Plume observations from two oil and gas sites in the Western Siberian Lowlands near Pangody, RU. The northern plume (denoted by the redbox) was observed on 12/03/2024 at 09:47:13 at an estimated rate of $1,873 \pm 917$ kg CH₄ hr⁻¹. The plumes in the southeast of the figure were observed on 20/04/2024 at 09:30:59 at an estimated rate of $2,694 \pm 1,050$ kg CH₄ hr⁻¹ and $4,596 \pm 1,792$ kg CH₄ hr⁻¹. The impact of the river on the southern plume is evident with no methane concentration for those pixels. Background image is PlanetScope panchromatic (band 8). Includes copyrighted material of GHGSat All rights reserved. Includes copyrighted material of Planet Labs PBC. All rights reserved.

3.1 Updated priors:

165

170

175

Our probabilistic emissions increased the oil and gas prior by 4.48 Tg CH₄ yr⁻¹ in the domain with emissions from 452 facilities, with 158 of these within our domain (Figure 1). The GFEI v2.0 estimates coinciding with the GHGSat observation sites were 3.973 × 10⁵, 3.2101 x 10⁶, and 2.4 x 10² kg CH₄ yr⁻¹ for site 1, site 2, and site 3, respectively. If scaled to annual values (assuming year-round flux), the GHGSat observation estimates for each site are 9.4458 × 10⁷, 1.355 × 10⁶, and 2.0044 × 10⁷ kg CH₄ yr⁻¹ for site 1, site 2, and site 3, respectively. Sites 1 and 3 were orders of magnitude larger than the GFEI estimates. To calculate the likelihood of emission occurrence, we first identified the number of oil and gas facilities within each site's satellite observations footprint. The oil and gas facilities at each site were 18, 27, and 6 for site 1, 2, and 3, respectively. The oil and gas facilities per site were then used to calculate rate of occurrence (Eq. 2):

$$Rate \ of \ occurrence = \frac{\# \ of \ observed \ plumes}{Total \ Facilities*Total \ Observations}, \tag{2}$$



180

185

190



The calculation resulted in occurrence rates for each site of 0.93%, 0.93%, and 21.2%, which we averaged resulting in 7.7 ± 11.7% likelihood of occurrence across the three sites. If a single rate of occurrence is calculated for all sites the occurrence rate falls to 2.8%. Emission and error terms were calculated from the GHGSat plume emission and error estimates resulting in CH₄ emission values of 7,541.8± 25,767.3 Kg hr⁻¹ and CH₄ emissions error of 0 ± 9,077.8 Kg hr⁻¹. Following the propagation of these error terms using equation 1, we found a mean of 0.22 Kg s⁻¹ and standard deviation of 1.12 Kg s⁻¹. According to the GFEI v2.0, oil and gas emissions are 0.57 Tg CH₄ yr⁻¹ within our study region (Scarpelli et al. 2022). The likelihood calculation was then applied to all flaring locations, resulting in 56.6% of the 869 facilities having modelled annual emissions greater than zero. In the IMI domain, 158 of the 305 flaring detections had emissions. These updated emissions estimates resulted in a 4.48 Tg CH₄ yr⁻¹ estimate of plume emissions in the domain and a total prior emission estimate of 7.2 Tg CH₄ yr⁻¹. Our updated prior resulted in a significant increase in oil and gas emissions.

3.2 IMI emissions and performance:

Our updated prior increased total prior emissions from 2.7 Tg CH₄ yr⁻¹ to 7.2 Tg CH₄ yr⁻¹. The updated model resulted in a total posterior emission estimate of 2.98 Tg CH₄ yr⁻¹ (2.92-3.18 Tg CH₄ yr⁻¹). The default scenario had a slightly lower total posterior emission estimate of 2.71 Tg CH₄ yr⁻¹ (2.64- 2.91 Tg CH₄ yr⁻¹). The total posterior estimates were very similar, given they used the same TROPOMI data as an atmospheric constraint (Figure 4). However, the posterior estimates were outside the each other's uncertainty. The wetland CH₄ prior in both IMI models was 2.23 Tg CH₄ yr⁻¹. The posterior wetland emissions in the default model fell slightly to 2.22 Tg CH₄ yr⁻¹. In contrast, the run using the updated GHGSat priors resulted in the posterior wetland emission falling to 1.6 Tg CH₄ yr⁻¹ (Figure 4).



205

210



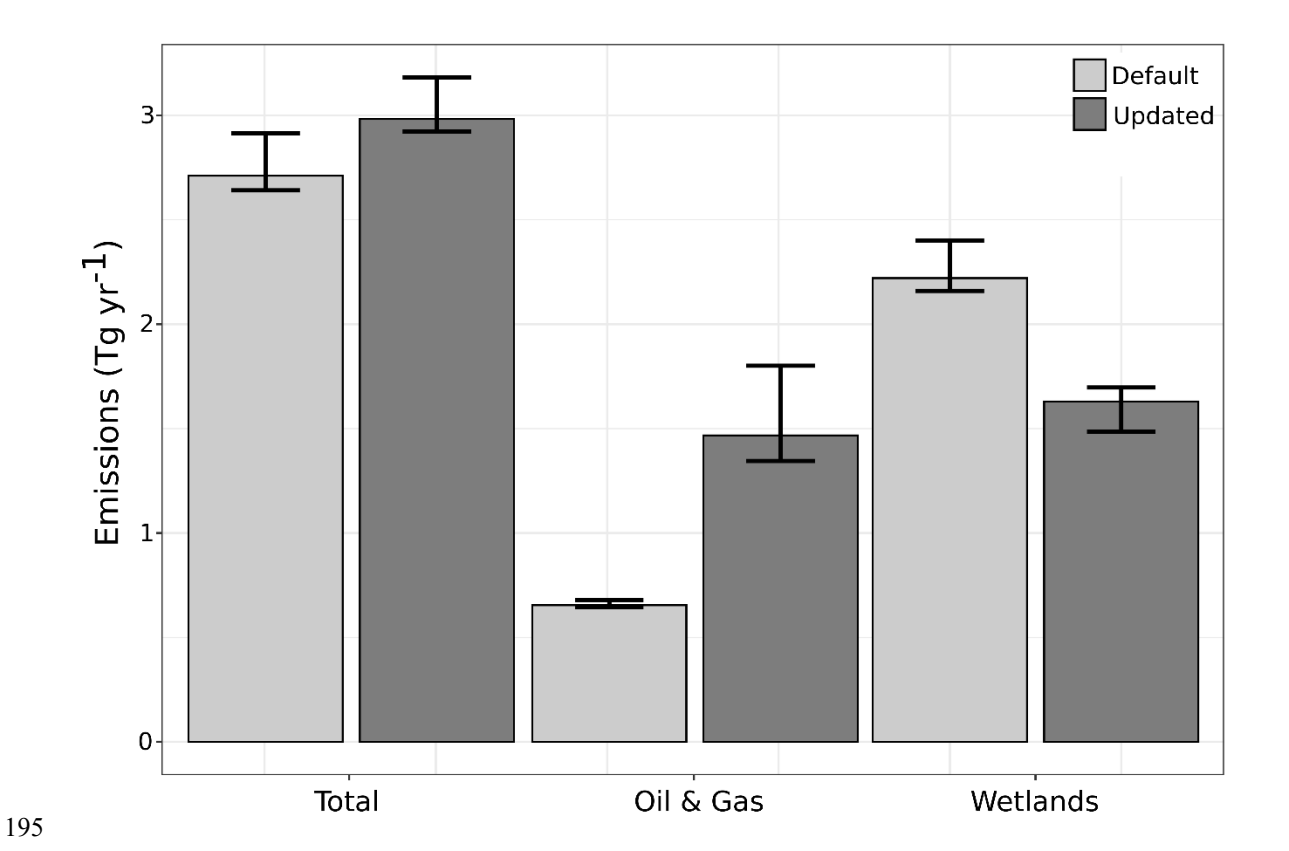


Figure 4. Posterior flux estimates for total emissions, oil and gas, and wetlands from both default and updated model runs, scaled to represent annual totals. Values scaled to the actual model run period (June 1, 2021 to July 31, 2021) are shown in Figure S4.

The updated model's higher prior emissions resulted in an increase in degrees of freedom. The posterior estimate from the inversion using the GHGSat updated priors had a slightly larger negative bias when comparing the posterior simulated CH4 concentrations from GEOS-Chem to observed XCH4 from TROPOMI (Table 1). Both models had improved performance in the posterior RMSE compared to the prior RMSE. For our domain there were 35,906 super-observations, representing 121,591 TROPOMI XCH4 observations. The averaging kernel sensitivity demonstrates that a few of our GHGSat informed priors are in locations that are unlikely to have emissions of that magnitude, which results in very low-scale factors. The major difference in the two models is the large northern regions which have the high scale factors in the default model and lower scale factors in the updated model. The updated model's inclusion of fugitive emissions in these regions results in 1) lower scale factors and 2) less of the increase in emissions from the region attributed to wetlands (Figure 4). Both models agree that a low scale factor is appropriate for the southern portion of the domain (Figure 5). This information could be used to update the distribution of our emission estimates and improve the updated model's performance. Low averaging kernel sensitivities approaching zero demonstrate where the model lacks TROPOMI XCH4 observations to constrain the forward model (Figure 5). Portions of the model domain had low sensitivity due to a lack of TROPOMI observations, which is a major uncertainty of this approach in regions with extensive wetlands and waterbodies.





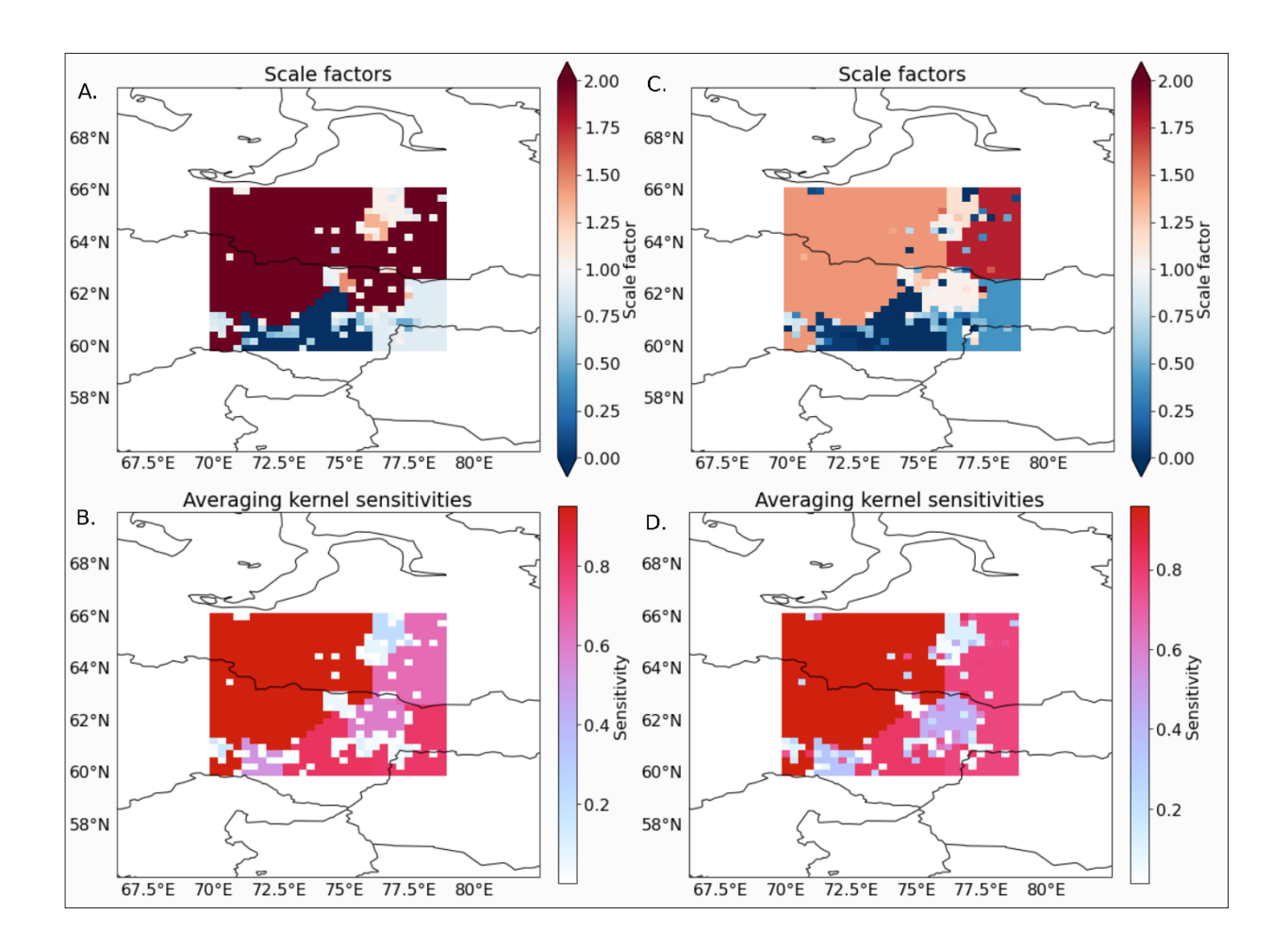


Figure 5: A. The scaling factors for the default model. B. the averaging kernel sensitivities for the default model. C. Scaling factors for the updated model. D. the averaging kernel sensitivities for the updated model.

Table 1. The mean bias and RMSE for the default and updated model runs. Values are calculated by comparing the GEOS-Chem atmospheric column CH₄ concentrations to the observed TROPOMI XCH₄ (Figure S5-S6).

Metric	Default (ppb)	Updated (ppb)
Bias in prior	-7.15 ppb	-3.38 ppb
Bias in posterior	-4.43 ppb	-4.78 ppb
RMSE prior	15.95 ppb	15.67 ppb





RMSE posterior	14.84 ppb	15.11 ppb
Degrees of Freedom	6.2	33.7

4 Discussion

220

225

230

235

240

The bias and RMSE are calculated by comparing simulated CH₄ concentrations based on the prior emissions estimates to the observed TROPOMI CH₄ concentrations and simulated CH₄ concentrations using the posterior emissions estimates to the observed TROPOMI CH₄ concentrations for the domain. The bias indicates that both prior and posterior GEOS-Chem model outputs were lower across the region than the TROPOMI XCH₄ observations (Table 1). The posterior simulations using the default and updated prior emissions estimates had similar biases of -4.43 ppb and -4.78 ppb, respectively. The lowest bias was found between the prior GEOS-Chem simulation using the GHGSat and OGIM updated priors and the observed XCH₄ from TROPOMI. The failure of the inversion to improve on this in the posterior model suggests a disconnect between the spatial distribution of our updated priors and the TROPOMI XCH₄ observations. The modelled emissions were consistently biased lower than the TROPOMI observations suggesting that additional emissions are feasible.

The posterior wetland emission estimates from the default and updated inversions were 2.22 and 1.63 Tg CH₄ yr⁻¹, respectively. The GHGSat informed priors resulted in a reduction of 0.59 Tg CH₄ yr⁻¹ attributed to wetlands. To put this in global context, this potential reduction represents 9.8% of the increase in CH₄ emissions attributed to wetlands in 2020 (6.0 ± 2.3 Tg CH₄ yr⁻¹; Peng et al. 2022). The prior emissions estimates for oil and gas informed using additional high-resolution observations affect wetland posterior emission estimates illustrating the potential of plume mappers to constrain wetland emission estimates in areas where the sources are closely co-located. Our approach was limited by 1) an overestimation of the magnitude of the updated prior which was adjusted for by the atmospheric constraint, 2) uncertainty of the spatial distribution of new emissions. Our approach demonstrates potential but needs more data to reduce the uncertainty.

4.1 Uncertainty:

Our modelling approach has several major uncertainties. The GHGSat informed priors are based on limited data from three sites across a region with extensive oil and gas facilities. It is possible that our observation sites are not representative of the region's oil and gas infrastructure. For example, only one of our three observation sites had detected flaring in the OGIM database. Additionally, less flaring has been linked to increased venting of excess gas (Irakulis-Loitxate et al. 2022), therefore, the flaring detections may underestimate potential emission sites and represent sites with consistent flaring but limited emissions. Pipelines are another source of fugitive emissions and were not included in our distribution of emissions. Additionally, our approach assumes consistent emissions across time, but fugitive emissions are sporadic and unpredictable



245

250

260

265



in length and timing. In the Permian basin, on average 26% of plumes were found to be persistent across multiple airborne deployments from September to November 2019 (Cusworth et al. 2021). Ideally, repeat coverage of the entire study domain would be available to determine plume persistence. However, regional plume observations are not available at the sensitivity of GHGSat. The IMI scaling factors are another uncertainty, optimized for only the period of interest from 06/01/2021 to 07/31/2021 but we use these values in calculating estimated emissions for the year. Running the model for the entire year would reduce this uncertainty. Shen et al. suggest that the low number of TROPOMI XCH₄ observations at high latitudes increased uncertainty in Russian inversions and that the GFEI 2.0 inventory underreported Russian emissions by a factor of two (2023). The posterior oil and gas estimate from the inversion using the updated oil and gas priors does represent approximately a doubling of the oil and gas emissions compared to the default inversion (0.65 Tg CH₄ yr⁻¹ to 1.47 Tg CH₄ yr⁻¹). Additionally, the default wetland and fossil priors are from 2017 and 2019, respectively, leading to some expected discrepancies between the modelled concentrations and TROPOMI XCH₄ observations in 2021.

255 **4.2 Distribution of update priors:**

To propose an improved approach to spatialize and update plume derived priors we analysed annual 2021 TROPOMI XCH₄ in relation to ancillary data including the Global Impervious Surface Area (GISA-10m; Huang et al. 2022) and GLWD 2.0 (Lehner et al. 2024). We analysed average TROPOMI XCH₄ for 2021 by percent impervious surface and percent wetland bins of 0-10, 10-20, 20-30, 30-40, 40-50, 50-60, 60-70, 70-80, 80-90, 90-100 and considering if the pixel fell within a gas field. We found that XCH₄ as observed by TROPOMI increased with impervious surface and decreased with wetland extent with both relationships being more pronounced in gas fields. The strong relationship of impervious surface to increased XCH₄ in the region does suggest that with additional refinement, impervious surface data could be more suitable than flaring to inform the spatial distribution of the updated priors. However, oil and gas infrastructure related disturbance has been identified as a driver of natural CH₄ emission hotspots (Sabrekov et al. 2022), which may contribute to the increasing TROPOMI XCH₄ relative to percent impervious surface.



275



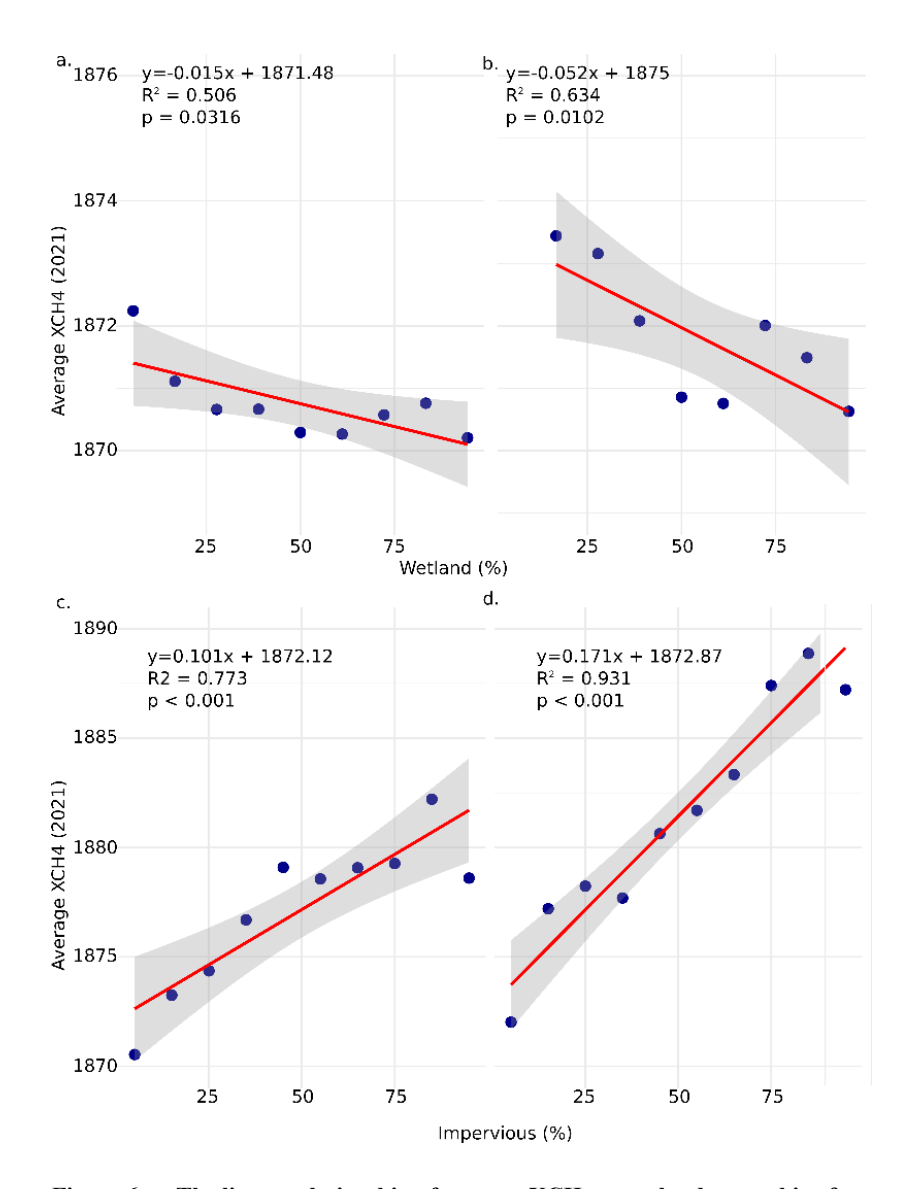


Figure 6: a. The linear relationship of average XCH₄ to wetland extent bins for non-gas fields. b. The linear relationship of average XCH₄ to wetland extent bins for gas fields. c. The linear relationship of average XCH₄ to impervious surface extent bins for non-gas fields. d. The linear relationship of average XCH₄ to impervious surface extent bins for gas fields.

Still, our work demonstrates the potential for improved modelling of CH₄ emissions from natural sources by incorporating plume-based mapping measurements in prior emission estimates. Oil and gas inventories for the region do disagree considerably by up to an order of magnitude (Scarpelli et al. 2022). Disagreement between GFEI v2.0 and Climate TRACE suggests that depending on tracking methodology, oil and gas emissions could be higher in the region. Still, our updated oil and gas priors are relatively high and would represent approximately 32% of Russian emissions for 2022 (Reuland et al. 2024). The latest version of GFEI demonstrated that the magnitude of methane plume mappers poorly correlate with the GFEI 3.0 emission estimates (Scarpelli et al. 2025).



280

285

290

295

300

305



4.3 Satellite Remote Sensing of Methane Plumes:

Fugitive emissions contribute to the uncertainty of emissions in the WSL. Plume mapping satellites are beginning to address this data gap (Jacob et al. 2022). The satellites with the capability to map plumes include NASA EMIT, GaoFen-5, GHGSat, Worldview-3, Sentinel-2 constellation, MethaneSat, TROPOMI, and Carbon Mapper. However, the use of these satellites for mapping plumes is limited by data access due to cost, expertise necessary for plume detection and emissions estimation, data processing, and sensor and mission limitations. For example, the WSL have limited collections from freely available datasets due in part to the low albedo in the SWIR of the peatland landscape limiting returns from coarse resolution satellite sensors and the high latitude limiting acquisitions from EMIT which is on the ISS. In contrast, we found GHGSat plume observations were minimally impacted by wetlands and waterbodies in the WSL (Figure 3). The GHGSat constellations did have a blackout season with no observations between approximately November 2023 and February 2024; for example, the last acquisition in the fall of 2023 was 02/11/2023 and the first in 2024 was 12/02/2024. These observations were for the WSL 2 site (61.3° N), with the higher latitude sites (65.8° N) having no observations in November or February (Table S2).

Earth observation solutions for improved monitoring of the WSL lowlands are currently limited. The SRON (Netherlands Institute of Space Research) plume dataset (Schuit et al. 2023) used TROPOMI data to map CH₄ plumes and found 18 plumes in our domain for 2021. The smallest was 4,000 kg CH₄ hr⁻¹, which is larger than all but three of the GHGSat detected plumes (Figure S7). The mean emission rate of the GHGSat plume data was 5.2 times less than the SRON data. It is evident that consistent small emissions from oil and gas infrastructure in the WSL are the common in our study sites and are not picked up by the plume mapping approach of the SRON dataset due to the spatial resolution and detection threshold of TROPOMI. While these emissions should be represented in the TROPOMI XCH₄ data, the limited returns in wetland, permafrost, and water pixels impacts the robustness of these data in regions like the WSL, making accurate inventory data critical for these locations. The sensitivity of the GHGSat observations (~100-200 kg hr⁻¹) and high spatial resolution (~30 m) is crucial for this region, as it allows for the observation of smaller fugitive emitters that are interspersed with wetland environments.

Ideally, daily plume estimates for the entire region would be available and utilized to update oil and gas prior emission estimates. However, given the limited current data, our methodology uses plume emission data to improve estimates of wetland emissions. We considered using SRON's plume data to provide a regional estimate of plume occurrence but the instruments' differing sensitivities to CH₄ concentration, complicates combining the two for improved estimation of the frequency of plumes across the region. While SRON's mapping effort examines mean emissions across the entire region, the super emitters observed are different from the smaller but persistent plumes observed by our study's GHGSat observations. Additional GHGSat images and other satellite data sources would improve our GHGSat informed priors' spatial distribution and emission estimates.

https://doi.org/10.5194/egusphere-2025-5398 Preprint. Discussion started: 26 November 2025

© Author(s) 2025. CC BY 4.0 License.





4.4 IMI and future work:

The development of the IMI is an ongoing process, with v2.0 and v2.2 being released during our study. This new versions incorporate features that are directly relevant to our work, such as plume measurements from SRON (Schuit et al. 2023) and additional tolerance for TROPOMI XCH₄ data over water. We used v1.2.1 of the IMI to test the use of GHGSat informed priors in a stable modelling environment. The benefits of water tolerance are significant, given that 13% of our domain is potentially water, as calculated from the global maximum extent surface water layer (Pekel et al. 2016). The gaps in TROPOMI XCH₄ observations due to water and wetlands limit the ability of the IMI to constrain the forward model outputs in those locations (Figure S8). This results in the inversion defaulting to the prior emission estimates in affected state vector elements, emphasizing the importance of accurate prior emission estimates from oil and gas.

IMI research so far has focused on utilizing analytical inversions to constrain fossil emissions at regional to global scales (Shen et al. 2023; Zhang et al. 2020). The utility of the approach is clear, however, the utilization of the IMI for improving our understanding of wetland environments has been limited but impactful (He et al. 2025). Utilizing GHGSat, we observed three locations in the WSL, finding consistent plume emissions at the observed facilities. We updated regional prior emission estimates with existing data on oil and gas infrastructure and plume emissions to constrain wetland emissions in the WSL. If oil and gas facilities across the domain had similar emissions to those observed with GHGSat, then less wetland emissions are likely to have occurred in this region during the study period. As additional satellites launch and more plume emission data are collected, we increase our ability to improve the accuracy of inverse modelling of atmospheric methane concentrations and reduce uncertainty in global wetland emission estimates.

Acknowledgments

This work utilized data made available through the NASA Commercial Satellite Data Acquisition (CSDA) program. The CSDA supported this work as part of the data on-ramp and evaluation process.

330 Open Research

320

325

GHGSat derived data necessary to reproduce this work are available in the supporting information (Table S2). All other data and software are freely available including TROPOMI XCH₄ (Copernicus Sentinel-5P, 2021). No new software or code was developed for this work.





335 References

- Bloom, A.A., Bowman, K.W., Lee, M., Turner, A.J., Schroeder, R., Worden, J.R., Weidner, R., McDonald, K.C. and Jacob, D.J., 2017. A global wetland methane emissions and uncertainty dataset for atmospheric chemical transport models (WetCHARTs version 1.0). *Geoscientific Model Development*, 10(6), pp.2141-2156.
- Brandt, A.R., Heath, G.A., Kort, E.A., O'Sullivan, F., Pétron, G., Jordaan, S.M., Tans, P., Wilcox, J., Gopstein, A.M., Arent, D. and Wofsy, S., 2014. Methane leaks from North American natural gas systems. *Science*, *343*(6172), pp.733-735.
 - Conrad, B.M., Tyner, D.R. and Johnson, M.R., 2023. The Futility of Relative Methane Reduction Targets in the Absence of Measurement-Based Inventories. *Environmental Science & Technology*, 57(50), pp.21092-21103.
- Copernicus Sentinel-5P (processed by ESA), 2021, TROPOMI Level 2 Methane Total Column products. Version 02. European Space Agency. https://doi.org/10.5270/S5P-3lcdqiv
 - Cusworth, D.H., Duren, R.M., Thorpe, A.K., Olson-Duvall, W., Heckler, J., Chapman, J.W., Eastwood, M.L., Helmlinger, M.C., Green, R.O., Asner, G.P. and Dennison, P.E., 2021. Intermittency of large methane emitters in the Permian Basin. *Environmental Science & Technology Letters*, 8(7), pp.567-573.
- Duren, R.M., Thorpe, A.K., Foster, K.T., Rafiq, T., Hopkins, F.M., Yadav, V., Bue, B.D., Thompson, D.R., Conley, S., Colombi, N.K. and Frankenberg, C., 2019. California's methane super-emitters. *Nature*, *575*(7781), pp.180-184.
 - Etiope, G., Ciotoli, G., Schwietzke, S. and Schoell, M., 2019. Gridded maps of geological methane emissions and their isotopic signature. *Earth System Science Data*, 11(1), pp.1-22.
- Fung, I., John, J., Lerner, J., Matthews, E., Prather, M., Steele, L. P., and Fraser, P. J.: Three-dimensional model synthesis of the global methane cycle, J. Geophys. Res.-Atmos., 96, 13033–13065, https://doi.org/10.1029/91JD01247, 1991.
 - He, Z., Gao, L., Liang, M. and Zeng, Z.C., 2024. A survey of methane point source emissions from coal mines in Shanxi province of China using AHSI on board Gaofen-5B. *Atmospheric Measurement Techniques*, 17(9), pp.2937-2956.
- He, M., Jacob, D.J., Estrada, L.A., Varon, D.J., Sulprizio, M., Balasus, N., East, J.D., Penn, E., Pendergrass, D.C., Chen, Z. and Mooring, T.A., 2025. Attributing 2019-2024 methane growth using TROPOMI satellite observations. *Authorea Preprints*.
 - Henze, D.K., Hakami, A. and Seinfeld, J.H., 2007. Development of the adjoint of GEOS-Chem. *Atmospheric Chemistry and Physics*, 7(9), pp.2413-2433.
 - Huang, X., Yang, J., Wang, W. and Liu, Z., 2022. Mapping 10-m global impervious surface area (GISA-10m) using multi-source geospatial data. *Earth System Science Data Discussions*, 2022, pp.1-39.
- Irakulis-Loitxate, I., Guanter, L., Maasakkers, J.D., Zavala-Araiza, D. and Aben, I., 2022. Satellites detect abatable superemissions in one of the world's largest methane hotspot regions. *Environmental science & technology*, 56(4), pp.2143-2152.
- Jacob, D.J., Varon, D.J., Cusworth, D.H., Dennison, P.E., Frankenberg, C., Gautam, R., Guanter, L., Kelley, J., McKeever, J., Ott, L.E. and Poulter, B., 2022. Quantifying methane emissions from the global scale down to point sources using satellite observations of atmospheric methane. *Atmospheric Chemistry and Physics*, 22(14), pp.9617-9646.



380

385

390



- Janssens-Maenhout, G., Pagliari, V., Guizzardi, D. and Muntean, M., 2013. Global emission inventories in the emission database for global atmospheric research (EDGAR)–Manual (I). *Gridding: EDGAR emissions distribution on global gridmaps, Publications Office of the European Union, Luxembourg*, 775.
- Jervis, D., McKeever, J., Durak, B.O., Sloan, J.J., Gains, D., Varon, D.J., Ramier, A., Strupler, M. and Tarrant, E., 2021. The GHGSat-D imaging spectrometer. *Atmospheric Measurement Techniques*, *14*(3), pp.2127-2140.
 - Lauvaux, T., Giron, C., Mazzolini, M., d'Aspremont, A., Duren, R., Cusworth, D., Shindell, D. and Ciais, P., 2022. Global assessment of oil and gas methane ultra-emitters. *Science*, *375*(6580), pp.557-561.
 - Lehner, Bernhard, Mira Anand, Etienne Fluet-Chouinard, Florence Tan, Filipe Aires, George H. Allen, Pilippe Bousquet et al. "Mapping the world's inland surface waters: An update to the Global Lakes and Wetlands Database (GLWD v2)." *Earth System Science Data Discussions* 2024 (2024): 1-49.
 - Lorente, A., Borsdorff, T., Butz, A., Hasekamp, O., Aan De Brugh, J., Schneider, A., Wu, L., Hase, F., Kivi, R., Wunch, D. and Pollard, D.F., 2021. Methane retrieved from TROPOMI: Improvement of the data product and validation of the first 2 years of measurements. *Atmospheric Measurement Techniques*, 14(1), pp.665-684.
 - Lin, H., Jacob, D.J., Lundgren, E.W., Sulprizio, M.P., Keller, C.A., Fritz, T.M., Eastham, S.D., Emmons, L.K., Campbell, P.C., Baker, B. and Saylor, R.D., 2021. Harmonized Emissions Component (HEMCO) 3.0 as a versatile emissions component for atmospheric models: application in the GEOS-Chem, NASA GEOS, WRF-GC, CESM2, NOAA GEFS-Aerosol, and NOAA UFS models. *Geoscientific Model Development*, 14(9), pp.5487-5506.
 - McLinden, C.A., Griffin, D., Davis, Z., Hempel, C., Smith, J., Sioris, C., Nassar, R., Moeini, O., Legault-Ouellet, E. and Malo, A., 2024. An independent evaluation of GHGSat methane emissions: Performance assessment. *Journal of Geophysical Research: Atmospheres*, 129(15), p.e2023JD039906.
 - Omara, M., Gautam, R., O'Brien, M. A., Himmelberger, A., Franco, A., Meisenhelder, K., Hauser, G., Lyon, D. R., Chulakadabba, A., Miller, C. C., Franklin, J., Wofsy, S. C., and Hamburg, S. P.: Developing a spatially explicit global oil and gas infrastructure database for characterizing methane emission sources at high resolution, Earth Syst. Sci. Data, 15, 3761–3790, https://doi.org/10.5194/essd-15-3761-2023, 2023.
- Pekel, J.F., Cottam, A., Gorelick, N. and Belward, A.S., 2016. High-resolution mapping of global surface water and its long-term changes. *Nature*, *540*(7633), pp.418-422.
 - Peng, S., Lin, X., Thompson, R.L., Xi, Y., Liu, G., Hauglustaine, D., Lan, X., Poulter, B., Ramonet, M., Saunois, M. and Yin, Y., 2022. Wetland emission and atmospheric sink changes explain methane growth in 2020. *Nature*, 612(7940), pp.477-482.
- 400 R Core Team (2021). R: A language and environment for statistical computing. R Foundation for Statistical Computing, Vienna, Austria. URL https://www.R-project.org/.
 - Randerson, J. T., van der Werf, G. R., Giglio, L., Collatz, G. J., and Kasibhatla, P. S.: Global Fire Emissions Database, Version 4.1 (GFEDv4), ORNL DAAC, Oak Ridge, Tennessee, USA, https://doi.org/10.3334/ORNLDAAC/1293, 2018.



420

435



- Reuland, F., Puthuparambil, S., Kumble, S., Kirk, T., Muralidharan, R., Rabbani, M., Ayandele, E., Diaz, K., Wang, R., Owens, L., and Gordon, D.: Oil and gas, version 1: oil and gas production and refining, the Rocky Mountain Institute (RMI), Boulder, Colorado, USA, Climate TRACE Emissions Inventory [data set], https://climatetrace.org (last access: 09 September 2024), 2024.
- Rosentreter, J.A., Borges, A.V., Deemer, B.R., Holgerson, M.A., Liu, S., Song, C., Melack, J., Raymond, P.A., Duarte, C.M., Allen, G.H. and Olefeldt, D., 2021. Half of global methane emissions come from highly variable aquatic ecosystem sources. *Nature Geoscience*, 14(4), pp.225-230.
 - Rößger, N., Sachs, T., Wille, C., Boike, J. and Kutzbach, L., 2022. Seasonal increase of methane emissions linked to warming in Siberian tundra. *Nature Climate Change*, 12(11), pp.1031-1036.
 - Sabrekov, A.F., Sabrekov, A.F., Filippov, I.V., Filippov, I.V., Dyukarev, E.A., Dyukarev, E.A., Zarov, E.A., Zarov, E.A., Kaverin, A.A., Kaverin, A.A. and Glagolev, M.V., 2022. Hot spots of methane emission in West Siberian middle taiga wetlands disturbed by petroleum extraction activities. *Environmental dynamics and global climate change*, *13*(3), pp.142-155.
 - Scarpelli, T. R., Jacob, D. J., Grossman, S., Lu, X., Qu, Z., Sulprizio, M. P., Zhang, Y., Reuland, F., Gordon, D., and Worden, J. R.: Updated Global Fuel Exploitation Inventory (GFEI) for methane emissions from the oil, gas, and coal sectors: evaluation with inversions of atmospheric methane observations, Atmos. Chem. Phys., 22, 3235–3249, https://doi.org/10.5194/acp-22-3235-2022, 2022.
 - Scarpelli, T.R., Roy, E., Jacob, D.J., Sulprizio, M.P., Tate, R.D. and Cusworth, D.H., 2025. Using new geospatial data and 2020 fossil fuel methane emissions for the Global Fuel Exploitation Inventory (GFEI) v3. *Earth System Science Data Discussions*, 2025, pp.1-23.
- Schuit, B.J., Maasakkers, J.D., Bijl, P., Mahapatra, G., Van den Berg, A.W., Pandey, S., Lorente, A., Borsdorff, T., Houweling, S., Varon, D.J. and McKeever, J., 2023. Automated detection and monitoring of methane superemitters using satellite data. *Atmospheric Chemistry and Physics Discussions*, 2023, pp.1-47.
 - Shindell, D., Sadavarte, P., Aben, I., Bredariol, T.D.O., Dreyfus, G., Höglund-Isaksson, L., Poulter, B., Saunois, M., Schmidt, G.A., Szopa, S. and Rentz, K., 2024. The methane imperative. Frontiers in Science, 2, p.1349770.
- Sheng, Y., Smith, L.C., MacDonald, G.M., Kremenetski, K.V., Frey, K.E., Velichko, A.A., Lee, M., Beilman, D.W. and Dubinin, P., 2004. A high-resolution GIS-based inventory of the west Siberian peat carbon pool. *Global Biogeochemical Cycles*, 18(3).
 - Shen, L., Jacob, D.J., Gautam, R., Omara, M., Scarpelli, T.R., Lorente, A., Zavala-Araiza, D., Lu, X., Chen, Z. and Lin, J., 2023. National quantifications of methane emissions from fuel exploitation using high resolution inversions of satellite observations. *Nature Communications*, 14(1), p.4948.
 - Sherwin, E.D., El Abbadi, S.H., Burdeau, P.M., Zhang, Z., Chen, Z., Rutherford, J.S., Chen, Y. and Brandt, A.R., 2024. Single-blind test of nine methane-sensing satellite systems from three continents. *Atmospheric Measurement Techniques*, 17(2), pp.765-782.



450

455



- Serikova, S., Pokrovsky, O.S., Laudon, H., Krickov, I.V., Lim, A.G., Manasypov, R.M. and Karlsson, J., 2019. High carbon emissions from thermokarst lakes of Western Siberia. *Nature Communications*, 10(1), p.1552.
 - Solazzo, E., Crippa, M., Guizzardi, D., Muntean, M., Choulga, M. and Janssens-Maenhout, G., 2021. Uncertainties in the Emissions Database for Global Atmospheric Research (EDGAR) emission inventory of greenhouse gases. *Atmospheric Chemistry and Physics*, 21(7), pp.5655-5683.
- Spiess A (2018). propagate: Propagation of Uncertainty. R package version 1.0-6, https://CRAN.R-project.org/package=propagate.
 - Suslov, N.I., Kryukov, V.A., Markova, V.M. and Churashev, V.N., 2019, June. Energy sector of Russia and Siberia: problems and prospects. In *Journal of Physics: Conference Series* (Vol. 1261, No. 1, p. 012035). IOP Publishing.
 - Thorpe, A.K., Green, R.O., Thompson, D.R., Brodrick, P.G., Chapman, J.W., Elder, C.D., Irakulis-Loitxate, I., Cusworth, D.H., Ayasse, A.K., Duren, R.M. and Frankenberg, C., 2023. Attribution of individual methane and carbon dioxide emission sources using EMIT observations from space. *Science advances*, 9(46), p.eadh2391.
 - United Nations Environment Programme and Climate and Clean Air Coalition (2021). Global Methane Assessment: Benefits and Costs of Mitigating Methane Emissions. Nairobi: United Nations Environment Programme.
 - Varon, D.J., Jacob, D.J., Sulprizio, M., Estrada, L.A., Downs, W.B., Shen, L., Hancock, S.E., Nesser, H., Qu, Z., Penn, E. and Chen, Z., 2022a. Integrated Methane Inversion (IMI 1.0): a user-friendly, cloud-based facility for inferring high-resolution methane emissions from TROPOMI satellite observations. *Geoscientific Model Development*, 15(14), pp.5787-5805.
 - Varon, D. J., Laestrada, W. D., and Jiawei, Z.: geoschem/integrated_methane_inversion: imi 1.0.0-beta.2 release (imi-1.0.0-beta.2), Zenodo [code], https://doi.org/10.5281/zenodo.6578547, 2022b.
- Zhang, Z., Poulter, B., Melton, J., Riley, W.J., Allen, G.H., Beerling, D.J., Bousquet, P., Canadell, J.G., Fluet-Chouinard, E., Ciais, P. and Gedney, N., 2024. Ensemble estimate of global wetland methane emissions over the period 2000-2020 (under open discussion).
 - Zhang, Z., Poulter, B., Feldman, A.F., Ying, Q., Ciais, P., Peng, S. and Li, X., 2023. Recent intensification of wetland methane feedback. *Nature Climate Change*, *13*(5), pp.430-433.
- Zhang, Y., Gautam, R., Pandey, S., Omara, M., Maasakkers, J.D., Sadavarte, P., Lyon, D., Nesser, H., Sulprizio, M.P., Varon, D.J. and Zhang, R., 2020. Quantifying methane emissions from the largest oil-producing basin in the United States from space. *Science advances*, 6(17), p.eaaz5120.